Nonequilibrium dynamics from BCS to the bosonic limit

G. Seibold[1] and J. Lorenzana[2]

[1]*Institut für Physik, BTU Cottbus-Senftenberg, PBox 101344, 03013 Cottbus, Germany*

[2]*Institute for Complex Systems, ISC-CNR, Dipartimento di Fisica, Universitá di Roma 'La Sapienza', Piazzale Aldo Moro 5, 00185 Roma, Italy*

(Received 6 April 2020; revised 21 July 2020; accepted 14 September 2020; published 5 October 2020)

Within the time-dependent Gutzwiller approximation applied to the negative-U Hubbard model, we investigate the dynamics of a superconductor after an interaction quench for different values of the final interaction from weak to strong coupling. The equilibrium BCS-BEC crossover becomes a sharp transition in the out-of-equilibrium dynamics between weak- and strong-coupling dynamical phases. Two different frequencies ($\Omega_J < \Omega_U$) dominate the order parameter dynamics. In the weak coupling phase, Ω_J follows twice the asymptotic average value of the gap ($\Omega_J \approx 2\Delta_\infty$) and Ω_U is much larger but hardy visible in the anomalous density. At long times the BCS dynamics is recovered but surprisingly differences remain during the transient phase. In the strong coupling phase, the dynamics decouples from the asymptotic value of the order parameter except at exactly half filling and close to the dynamical transition where $\Omega_U \approx 2\Delta_\infty$. The out-of-equilibrium transient spectral density and optical conductivity are presented and discussed in relation to pump probe experiments. Both Ω_J and Ω_U give rise to a complex structure of self-driven slow Rabi oscillations which are visible in the nonequilibrium optical conductivity where also sidebands appear due to the modulation of the double occupancy by superconducting amplitude oscillations. Analogous results apply to CDW and SDW systems. Our results show that in systems with long coherence times, pump-probe experiments allow us to characterize the regime (BCS vs preformed pairs) through very specific out-of-equilibrium fingerprints.

DOI: 10.1103/PhysRevB.102.144502

I. INTRODUCTION

During the past two decades rapid progress has been made in the study of ultracold fermionic quantum gases, in particular concerning the realization of a paired BCS state [1–3] where the interaction strength can be tuned via Feshbach resonances [4]. These systems provide a platform to investigate in a controlled way the coherent modes of superfluid systems like massive amplitude ("Higgs") or density modes and Goldstone phase excitations of the order parameter [5]. Also in condensed matter physics the detection of the superconducting amplitude mode and charge modes in real time has being the subject of intense research [6–8].

These experiments have motivated the analysis of the BCS pairing problem with time-dependent interactions and several proposals based on the realization of a suitable out-of equilibrium dynamics (pump) which is then measured by a probe pulse [9–15]. Within the pseudospin formulation of Anderson [16] the problem can be mapped onto an effective spin Hamiltonian for which the Bloch dynamics can be solved exactly [17–21].

In this weak coupling regime, the effect of a sudden change of the pairing interaction has been thoroughly studied. The dynamics of the Cooper pair states either dephases or synchronizes [19]. When the change in the attractive interaction is small or moderate (either increasing or decreasing), the dynamics is characterized by damped amplitude oscillations for small quenches with a final finite value of the order parameter. Instead, if the interaction is quenched below a critical value in magnitude, dephasing drives the pairing amplitude to zero. The synchronization regime occurs upon increasing the interaction beyond a critical value. In this case a self-sustained dynamical state is reached in which all Cooper pairs states oscillate with the same phase. Off course in the presence of damping the oscillations eventually decay [10].

The negative-U Hubbard model is a well established theoretical framework to study the crossover from the weak-coupling BCS limit to the strong-coupling limit of Bose-Einstein condensation (BEC) under equilibrium conditions (see Ref. [22] and references therein).

From the experimental side, due to the possible control of interparticle interactions with Feshbach resonances mentioned above, ultracold Fermi gases provide also an excellent platform to investigate the evolution from BCS to the BEC regime. In this context, the formation of molecular dimers composed of fermionic atoms, which corresponds to the realization of a BEC-type superfluid in the strong coupling limit, was reported in Refs. [23–26]. Subsequent experiments [1–3,26] then realized the crossover to a BCS-type system by variation of the coupling strength and the spectroscopic observation of the pairing gap [27,28] in this crossover regime. This platform allows us to also modulate the interaction in real time through the modulation of Feshbach resonances [4,29], opening the possibility to study the out-of-equilibrium dynamics of a condensate across the entire range of coupling strengths.

In this paper we use the attractive Hubbard model to investigate the dynamics of a fermionic condensate after a sudden

quench of the interaction parameter U and how it evolves from the BCS to a regime of preformed pairs which at low temperature in equilibrium would correspond to BEC. We use the time-dependent Gutzwiller approximation (TDGA) [30–40] in order to study the spectral properties of this model in the resulting nonequilibrium situations. It has been shown before that, in the linear response limit [31,34], this approach gives a very good account of charge [35], magnetic [36], and pairing [37,38] fluctuations as compared with exact diagonalization on small clusters and has been applied with success to the description of, for example, magnetic excitations in cuprate superconductors [41–43]. In fact, the TDGA includes the high-energy dynamics due to double occupancy fluctuations which are missing in the conventional time-dependent Hartree-Fock approximation. It is therefore a convenient and reliable approach for computing nonlocal correlations in inhomogeneous correlated systems which are much harder to access with dynamical mean-field theory [44] (DMFT). At the same time, it provides a reliable description of collective modes, for example spin waves in broken symmetry states [45] (equivalent to sound waves in superfluid systems), which are missing in single site DMFT. Also away from linear response [31–33] and despite the lack of true thermalization, the TDGA provides a good description [39,40] of the order parameter dynamics in the prethermal regimes and shows good agreement with nonequilibrium dynamical mean-field approximation [46–49].

The TDGA has been applied to investigate the dynamics of correlated paramagnetic states [32,33,50], order parameter dynamics of antiferromagnetism [39], and superconductivity [40,51] as a result of an interaction quench from an initial to a final Hubbard interaction ($U_i \to U_F$). Interestingly, this approach reveals the occurrence of a dynamical phase transition in the order parameter dynamics at a critical final interaction $U_F = U_c$ which depends on density and on U_i. The dynamical transition reflects in several features: (i) In contrast to the smooth crossover found at equilibrium, the transition at U_c is sharp and separates a 'weak' from a 'strong coupling' regime where the latter is characterized by a decreasing long-time averaged order parameter for increasing interaction strength whereas in the weak coupling regime the order parameter follows the quenched interaction similar to standard time-dependent Hartree-Fock theory. (ii) At U_c the minimum amplitude of the oscillating Gutziller renormalization factor approaches zero, thus revealing an underlying 'dynamical localization transition.' (iii) At U_c the conjugate phase of the double occupancy changes from oscillating around zero to a precession around the unit circle similar to an estonian swing.

Here, we study the strongly nonlinear dynamics that arises after a sudden change in the interaction. The dynamical transition manifests as a sharp anomaly in the long-time average of the gap which becomes a strong discontinuity at half filling. This is in contrast to the equilibrium gap which evolves smoothly in the whole range of coupling which is thus termed a "crossover." By analyzing the Fourier transform of the anomalous density or double occupancy, two main frequencies are identified in the dynamics, Ω_J and Ω_U with $\Omega_J < \Omega_U$. For final coupling strengths below the critical one the out-of-equilibrium dynamics of the anomalous density is BCS-like at long times. Indeed, the main oscillation has frequency Ω_J and coincides with twice the gap parameter at $t \to \infty$. The transient dynamics, however, considerably differs from the BCS dynamics. Above the critical coupling the dynamics changes dramatically, both frequencies become important and for large quenches they tend to decouple from the asymptotic gap except at exactly half filling.

We further demonstrate a nonlinear mechanism relevant at intermediate and strong coupling by which the above oscillations of macroscopic variables (like the double occupancy) originating from a quench, act back on the superconducting quasiparticles as a periodic drive. This produces self-sustained Rabi oscillations originating from the interplay between Ω_J and Ω_U excitations. Indeed, the TDGA can be viewed as an effective BCS model where the bandwidth is periodically driven by the macroscopic oscillating variables. In the latter case, Rabi oscillations have been demonstrated in Refs. [52,53]. We show how the frequencies Ω_J and Ω_U reveal themselves in the density of states (DOS) and optical conductivity. Because of the attractive-repulsive transformation [54] and the symmetry of the Hubbard model our results for superconductivity at half filling apply also to spin and charge-density-wave states.

The paper is organized as follows. In Sec. II A we give a brief derivation of the TDGA based on a time-dependent variational principle. We discuss the equilibrium phase diagram in Sec. II B. Section III is devoted to the analysis of the quench dynamics, also in comparison to the weak-coupling BCS limit. The appearance of self-sustained Rabi oscillations is demonstrated in Sec. IV while in Sec. V we show how these excitations reflect in the optical conductivity. We conclude our discussion in Sec. V.

II. FORMALISM

We study the attractive Hubbard model

$$H = \sum_{k,\sigma} \varepsilon_k c^\dagger_{k,\sigma} c_{k,\sigma} + U \sum_r n_{r,\uparrow} n_{r,\downarrow}, \tag{1}$$

where electrons with dispersion ε_k on a lattice (number of sites N) interact via a local attraction $U < 0$. We are interested in the dynamics after a quench in the interaction.

A. Equations of motion

The evolution is obtained variationally by means of the time-dependent Gutzwiller wave function

$$|\Psi_G\rangle = \hat{P}_G |BCS\rangle,$$

with $\hat{P}_G$ and $|BCS\rangle$ the time-dependent Gutzwiller projector and BCS state. The variational solution of the time-dependent Schrödinger equation can be obtained by requiring the action $S = \int dt L$ to be stationary with the following real Lagrangian [31]

$$L = \frac{i}{2} \frac{\langle \Psi_G | \dot{\Psi}_G \rangle - \langle \dot{\Psi}_G | \Psi_G \rangle}{\langle \Psi_G | \Psi_G \rangle} - \frac{\langle \Psi_G | H | \Psi_G \rangle}{\langle \Psi_G | \Psi_G \rangle} \tag{2}$$

which leads to the equations of motion from the standard Euler-Lagrange equations.

Equation (2) can be evaluated within the Gutzwiller approximation (GA) [31–33] where expectation values of $|\Psi_G\rangle$ can be expressed as renormalized expectation values of a (translationally invariant) BCS state. Superconductivity is then most conveniently incorporated [55,56] by (a) performing a rotation in charge space to a normal state, (b) applying the Gutzwiller approximation, and (c) rotating the density matrix back to the original frame (cf. Ref. [37]).

The Gutzwiller approximated expectation value of the Hamiltonian in Eq. (2) including a chemical potential term is given by

$$E^{\mathrm{GA}} = T_0 + T_1 - \mu N + UND, \tag{3}$$

$$T_0 = \sum_k q_\parallel \varepsilon_k [\langle c^\dagger_{k,\uparrow} c_{k,\uparrow}\rangle - \langle c_{-k,\downarrow} c^\dagger_{-k,\downarrow}\rangle + 1],$$

$$T_1 = \sum_k \varepsilon_k [q_\perp \langle c^\dagger_{k,\uparrow} c^\dagger_{-k,\downarrow}\rangle + q^*_\perp \langle c_{-k,\downarrow} c_{k,\uparrow}\rangle], \tag{4}$$

where $\langle\rangle$ denotes the $|BCS\rangle$ expectation value and we defined the double occupancy,

$$D = \langle \Psi_G | n_{r,\uparrow} n_{r,\downarrow} | \Psi_G \rangle,$$

and the regular (T_0) and anomalous (T_1) contribution to the kinetic energy. The anomalous contribution is a characteristic of the Gutzwiller approximation or the equivalent slave Boson formulation [56] and arises from the rotation in charge space applied to the kinetic term. The explicit form of the renormalization factors $q_\parallel$ and $q_\perp$ is given in Appendix A.

The dynamical variables of the problem are the density matrix,

$$\underline{\underline{R}}(k) = \begin{pmatrix} \langle c^\dagger_{k,\uparrow} c_{k,\uparrow}\rangle & \langle c^\dagger_{k,\uparrow} c^\dagger_{-k,\downarrow}\rangle \\ \langle c_{-k,\downarrow} c_{k,\uparrow}\rangle & \langle c_{-k,\downarrow} c^\dagger_{-k,\downarrow}\rangle \end{pmatrix},$$

the parameter D, and its conjugate phase η which vanishes in the GA equilibrium state. Stationarity of the Lagrangian leads to the following equations of motion [31–33],

$$\frac{d}{dt}\underline{\underline{R}}(k) = -i[\underline{\underline{R}}(k), \underline{\underline{H}}^{\mathrm{GA}}(k)] \tag{5}$$

$$\dot{D} = \frac{1}{N}\frac{\partial E^{\mathrm{GA}}}{\partial \eta} \tag{6}$$

$$\dot{\eta} = -\frac{1}{N}\frac{\partial E^{\mathrm{GA}}}{\partial D} \tag{7}$$

and the Gutzwiller Hamiltonian is evaluated from

$$H^{\mathrm{GA}}_{nm}(k) = \frac{\partial E^{\mathrm{GA}}}{\partial R_{mn}(k)}, \tag{8}$$

which is explicitly shown in Appendix B. Conservation of the energy $E^{\mathrm{GA}}(R, D, \eta)$ follows from

$$\frac{dE^{\mathrm{GA}}}{dt} = \sum_k \frac{\partial E^{\mathrm{GA}}}{\partial R_{nm}(k)} \dot{R}_{nm}(k) + \frac{\partial E^{\mathrm{GA}}}{\partial D}\dot{D} + \frac{\partial E^{\mathrm{GA}}}{\partial \eta}\dot{\eta}$$

$$= -i \sum_k Tr\{\underline{\underline{H}}^{\mathrm{GA}}(k)[\underline{\underline{R}}(k), \underline{\underline{H}}^{\mathrm{GA}}(k)]\} = 0$$

where the second and third term in the first line cancel because of Eqs. (6) and (7) and the first term vanishes upon permutating the trace.

It is convenient to introduce the charge spinor $\mathbf{J}_k$ with the components

$$J^x_k = \tfrac{1}{2}(\langle c^\dagger_{k,\uparrow} c^\dagger_{-k,\downarrow} + c_{-k,\downarrow} c_{k,\uparrow}\rangle), \tag{9}$$

$$J^y_k = -\tfrac{i}{2}(\langle c^\dagger_{k,\uparrow} c^\dagger_{-k,\downarrow} - c_{-k,\downarrow} c_{k,\uparrow}\rangle), \tag{10}$$

$$J^z_k = \tfrac{1}{2}(\langle c^\dagger_{k,\uparrow} c_{k,\uparrow} + c^\dagger_{-k,\downarrow} c_{-k,\downarrow}\rangle - 1). \tag{11}$$

We also define the expectation value of raising and lowering operators,

$$J^+_k = \langle c^\dagger_{k,\uparrow} c^\dagger_{-k,\downarrow}\rangle \tag{12}$$

$$J^-_k = \langle c_{-k,\downarrow} c_{k,\uparrow}\rangle. \tag{13}$$

Integrated global quantities will be denoted by dropping the momentum label, i.e., $J^\mu \equiv \sum_k J^\mu_k/N$, $J^2 \equiv (J^z)^2 + (J^x)^2 + (J^y)^2$. We will refer to the momentum integrated $J^\pm$ as the Gorkov function.

The dynamics of the density matrix, Eq. (5), can be equivalently expressed as Bloch equations for Anderson pseudospins,

$$\dot{\mathbf{J}}_k = 2\mathbf{b}_k \times \mathbf{J}_k \tag{14}$$

with an effective magnetic field

$$\mathbf{b}_k = -(\Delta'_k, \Delta''_k, q_\parallel(t)\varepsilon_k - \mu). \tag{15}$$

Here we defined the real (Δ'_k) and imaginary part (Δ''_k) of the spectral gap which is given by the off-diagonal element of the time-dependent Gutzwiller Hamiltonian $\Delta_k(t) \equiv H^{\mathrm{GA}}_{12}(k)$ [Eq. (A5)]. From Eq. (8) it is clear that $\Delta_k(t)$ is the conjugate field of the Gorkov function.

In contrast to the BCS case, in the Gutzwiller treatment the gap acquires a momentum dependence. This originates from the bare dispersion, appearing in T_1, which is directly related to H^{GA}_{12},

$$\Delta_k \equiv \Delta_\mu + q^*_\perp(\varepsilon_k - \mu/q_\parallel). \tag{16}$$

Here we separated Eq. (A5) into a momentum independent part Δ_μ and a momentum dependent part which (unlike a usual momentum-dependent gap) vanishes at the chemical potential (see Appendix A for details).

Once the system is taken out of equilibrium both Δ_μ, $q_\perp$ and $q_\parallel$ become time dependent. In particular, $q_\perp$ is related to fluctuations of the double occupancy phase $\delta\eta$ [cf. Eq. (A2)]. In the weak coupling limit fluctuations of the double occupancy phase $\delta\eta$ tend to vanish and one recovers the BCS momentum independent gap since $q_\perp \sim \delta\eta \to 0$. In this limit one also recovers the BCS relation $\Delta_\mu = UJ^-$. How the GA approaches the BCS results in the dynamical case is studied further in Sec. III B 1. The dynamics of the double occupancy $D(t)$ influences on the z component of $\mathbf{b}_k$ via the renormalization factor $q_\parallel(t)$ [Eq. (A1)] which will be an essential point in our analysis of Rabi oscillations in Sec. IV.

B. Static phase diagram

Before discussing the dynamics we would like to comment on the accuracy of our approximations regarding static quantities and recall the static phase diagram.

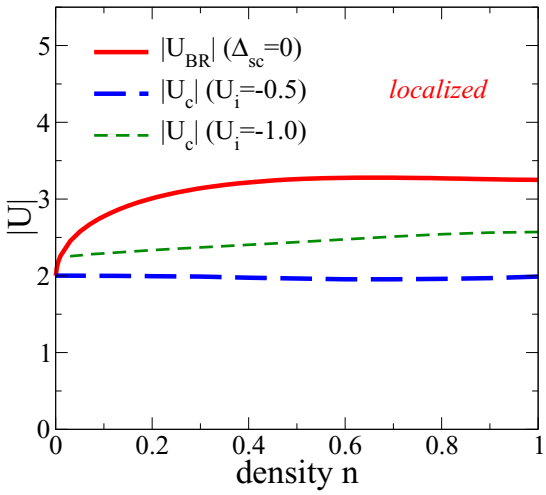

FIG. 1. Solid red: Brinkman-Rice transition ($q_\parallel = 0$) for the attractive, square lattice model in the Gutzwiller approximation restricted to a nonsuperconducting ground state. Energies are given in units of the half bandwidth $B = 1$. In the superconducting system a dynamical phase transition with vanishing $q_\parallel$ occurs upon quenching from an initial U_i to a final critical U_c. The dashed blue and green lines show U_c for $U_i = -0.5$ and $U_i = -1$, respectively.

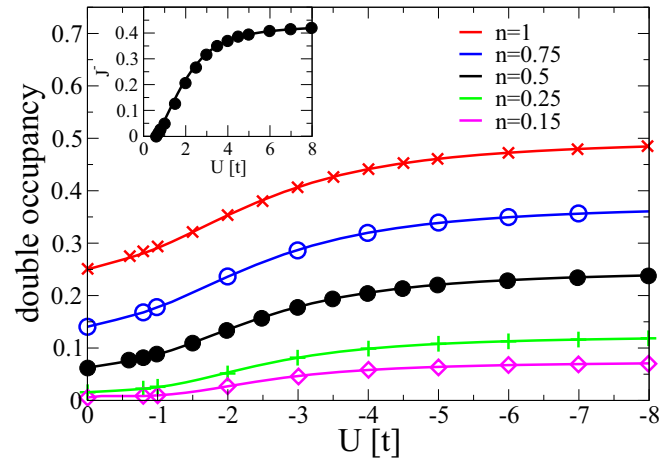

FIG. 2. Main panel: Symbols show the double occupation in dynamical mean-field theory in the SC broken symmetry phase as a function of U from Ref. [59]. Inset: U dependence of the Gorkov function for $n = 0.5$. The lines in both panels were obtained with the static GA. The underlying system is a Bethe lattice with bandwidth parameter $B = 2t$.

The Gutzwiller approximation for the *repulsive* Hubbard model restricted to a nonmagnetic ground state yields the well-known Brinkman-Rice transition [57] at a critical value of U where electrons localize due to the vanishing of the bandwidth renormalization factor *only at half filling*.

In case of the *attractive* model and restricting to a nonsuperconducting ground state also a localization transition is obtained, but now it appears at *each* density [55,56]. This is shown in Fig. 1 where the red line indicates the Brinkman-Rice U above which the ground state is localized.

The above phase diagram can be easily understood from the attractive-repulsive transformation [54] which maps the negative U-Hubbard model into a positive U-Hubbard model with a finite magnetization given by $(n-1)/2$. As is well known, in the Brinkman-Rice picture a Mott insulator is described as a collection of fully localized spin-1/2 fermions thus effectively neglecting the scale J of magnetic interactions. The Mott states of the negative U-Hubbard for arbitrary n can be seen as derivatives of the familiar half-filled positive U-Brinkman-Rice insulating state in which a certain number of spins have been flipped to produce a finite magnetization corresponding to $(n-1)/2 \neq 0$. Thus, for example, a positive U-Mott insulating state in which the magnetic configuration is a ferromagnet with a spin flip ($|\downarrow\downarrow \ldots \downarrow\uparrow\downarrow \ldots \downarrow\downarrow\rangle$) maps into a single composite boson localized at the site i of the flipped spin, i.e., the state $c^\dagger_{i,\downarrow} c^\dagger_{i,\uparrow}|0\rangle$ of the negative U model. Clearly, the Mott state reflects the formation of local pairs in the charge language and neglecting the magnetic exchange excitations in the positive U language is equivalent to neglecting the boson kinetic energy in the negative U language. Thus, the Brinkman-Rice transition reflects the transition to an incoherent state of preformed pairs which is a fair description of the system for large $|U|$ at a temperature less than $|U|$ but larger than the ordering temperature. One may argue that sharp transitions as the Brinkman-Rice transition do not reflect the physics of the Hubbard model. We come back to this point below.

Allowing for superconductivity (SC) at zero temperature, the Brinkman-Rice transition is avoided and replaced by the smooth BCS-BEC crossover in the stationary state. We anticipate that in a nonequilibrium situation a related dynamical transition appears near the critical value of the final interaction parameter U_F depending weakly on the initial value U_i. Thus, studying the dynamical behavior of the system one can in principle determine the regime (weak or strong coupling) of a given system.

Since the dynamics is based on the GA approximation it is worth it to analyze its quality in the static case with regard to other approaches. In Fig. 2 we compare the DMFT results from Ref. [59] in the SC broken symmetry state with the static GA approximation. One can see that there is almost perfect quantitative agreement between the two approaches. As mentioned before, the transition from weak to strong coupling at equilibrium is a crossover so there are no sharp features in the static quantities. Still, for all quantities there is a noticeable change of regime for $-U$ of the order of the bandwidth, i.e., in the range $-U \approx 2-4$, depending on doping. In the dilute limit, this corresponds to the point where the chemical potential is below the band, an unambiguous signal of the BEC regime. For general fillings, this criteria cannot be used as for example at half filling the chemical potential is pinned at $U/2$. Fortunately, the case of half filling can be directly mapped to the half-filled repulsive model which has being extensively studied with DMFT [44]. Suppressing long-range order, the system displays the well-known Mott transition from a metallic phase to the insulating phase with the concomitant formation of Hubbard bands which reflects a phase in which local magnetic moments have been formed but are not ordered. Clearly, in the attractive model, this corresponds to a phase of incoherent local pairs. As mentioned above,

the Brinkman-Rice transition also describes the transition to a phase of incoherent local pairs without off-diagonal long-range order. Remarkably, the transition point computed in the GA almost coincides [44] with the DMFT theory result which again shows the surprising accuracy of the GA even suppressing long-range order. Thus we conclude that in the present model, for general filling, the Brinkman-Rice transition point of the negative-U model marks the transition to the regime of local pair formation analogous to the nonmagnetic Mott phase of the repulsive model which physical significance is well understood. The fact that the GA accurately describes this transition at equilibrium supports the relevance of the present study concerning the out-of-equilibrium behavior of the SC attractive Hubbard model.

III. QUENCH DYNAMICS

We prepare the system in the GA equilibrium state for a given particle concentration n and initial interaction U_i. Then the interaction is instantaneously changed to a final value U_F and the resulting dynamics is studied within the formalism developed above. As discussed in the introduction, an interaction quench can in principle be realized in ultracold Fermi gases manipulating a Feshbach resonance. In the solid state, a sudden change of the interaction is not easy to implement. However, one can use a pump laser pulse to impose a nonequilibrium and nonthermal distribution of quasiparticles. While there is an infinite number of possible nonequilibrium distributions one expects that the evolution does not depend much on the details of the distribution but on integrated quantities as the injected excess energy. Indeed, a large portion of the weak-coupling BCS phase diagram (excluding the synchronization regime) the average gap at long times is close to the gap that would be obtained in a thermal distribution with the same injected energy [19]. Thus, a quench protocol allows us to study a family of nonequilibrium distributions controlled by a single parameter $\Delta U = U_i - U_F$ instead of the implementation of pulse shape, strength, and duration. We are of course assuming that the pulse duration is much shorter than the thermalization scales of the system. A discussion of how interaction ramps lead to differences with regard to the 'sudden' quench can be found in Ref. [40].

In order to study the effect of dimensionality we consider two systems: First, a Bethe lattice with infinite coordination number and density of states $\rho(\omega) = \frac{2}{\pi B^2}\sqrt{B^2-\omega^2}$ for which the Gutzwiller approximation becomes an exact evaluation of expectation values within the Gutzwiller wave function (which is of course still an approximate variational wave function). Second, a square lattice with nearest-neighbor hopping which is characterized by a density of states $\rho(\omega) = \frac{2}{\pi^2 B}\mathcal{K}(\sqrt{1-\omega^2/B^2})$ and $\mathcal{K}$ is the complete elliptic integral of the first kind. All energy scales will be defined with respect to $B \equiv 1$. In the main part of the paper we will show results for the square lattice and comment on differences to the dynamics of the Bethe lattice for which some results are shown in Appendix C. From now on, long-time averages of dynamical quantities $A(t)$ will be denoted by $\langle A\rangle_T$, i.e.,

$$\langle A\rangle_T = \lim_{t\to\infty}\frac{1}{T}\int_t^{t+T} A(t),$$

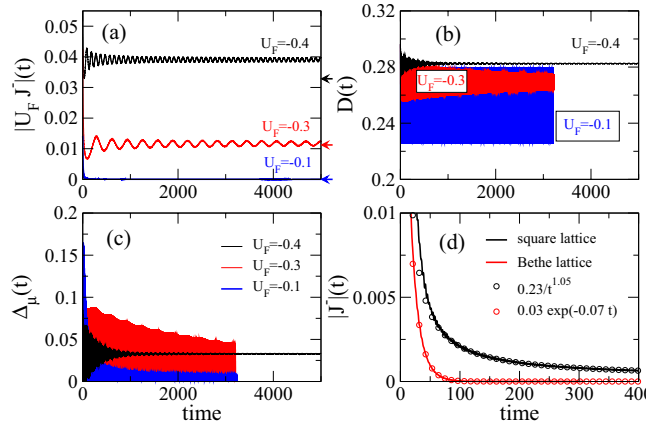

FIG. 3. Time dependence of the Gorkov function J^- [panels (a) and (d)], the double occupancy D [panel (b)], and the spectral gap parameter at the chemical potential $\Delta_\mu(t)$ [panel (c)] for a U quench from $U_i = -0.5$ to U_F with $|U_F| < |U_i|$. In panel (a) the Gorkov function is scaled with U_F in order to make comparison with the asymptotic value of $\Delta_\mu(t\to\infty)$ which is indicated by arrows on the right vertical axis. Results in (a)–(c) are for a half-filled square lattice whereas (d) compares the long time behavior of J^- between half-filled Bethe and square lattice for $U_F = -0.1$.

where T comprises a sufficiently large number of oscillations.

A. $|U_F| < |U_i|$ quench

For small quenches [cf. Fig. 3(a)], similar to the (linearized) BCS dynamics [20,21], the Gorkov function displays a power law, decaying, long-time behavior

$$J^-(t) = J^-_\infty[1+\alpha\cos(2\Delta_\infty t)/\sqrt{\Delta_\infty t}] \tag{17}$$

due to dephasing [58]. At weak coupling we will refer to the dominant frequency of the Gorkov function at long times as Ω_J. At strong coupling, other frequencies will appear in the Gorkov function but we will keep the denotation of Ω_J by continuity with the present weak-coupling regime.

It follows from Eq. (17) that

$$\Omega_J = 2\Delta_\infty \equiv 2\langle\Delta_\mu(t\to\infty)\rangle_T\,, \tag{18}$$

i.e., the frequency of J^- is determined by the long time limit of the spectral gap Δ_∞ at the chemical potential. Furthermore, we find that at long times, with a good approximation $UJ^-(t\to\infty) \approx \Delta_\mu(t\to\infty)$ which is a hallmark of BCS weak-coupling theory. This will be analyzed in more detail below for $|U_F| > |U_i|$ where one can tune the system from weak to strong coupling in $|U_F|$.

Panel (b) of Fig. 3 displays the dynamics of the double occupancy. Because the dominant frequency is much larger than for the Gorkov function, the main oscillation is not resolved and only the envelope is visible as the boundary of the colored regions. We will call the dominant frequency of the double occupancy Ω_U. In general $\Omega_U > \Omega_J$. For small U, Ω_U is determined [31] by the bandwidth while for large U is of order U. The intermediate behavior will be analyzed in detail below.

For the cases in which the Gorkov function oscillates and remains finite at long times (black and red), the dynamics

resembles two coupled oscillators with a fast frequency Ω_U and a slow frequency Ω_J. Indeed, the slow frequency of the Gorkov function Ω_J is also clearly visible in the envelope of the double occupancy evolution which shows that J^- and D are significantly coupled. On the other hand, since the natural dynamics of $J^-(t)$ is much slower it does not respond to the fast oscillation of $D(t)$ and therefore the fast oscillations are hardly visible in Fig. 3(a). Notice also that the relaxation of $D(t)$ and $J^-(t)$ occurs on the same time scale. In case of $J^-(t \to \infty) = 0$ (blue) one recovers the situation discussed in Refs. [32,33] where the double occupancy oscillates between the two extrema D_- and D_+ [upper and lower bounds of the blue curve in (b)].

Panel (d) of Fig. 3 shows the initial dynamics related to the vanishing of J^-. For some critical value of $|U_F| < |U_i|$ the Gorkov function dynamically vanishes and in this limit the decay from an initial J_i^- is described by the general asymptotic behavior derived in Ref. [21]

$$\frac{J^-(t)}{J_i^-} = A(t)e^{-2\alpha J_i^- t} + B(t)e^{-2J_i^- t}, \tag{19}$$

where $A(t)$ and $B(t)$ are decaying power laws $\sim 1/t^\nu$ with $1/2 \leqslant \nu \leqslant 2$ and $0 \leqslant \alpha \leqslant 1$. As shown in the figure, the decay in the 2D system follows a $1/t$ law whereas for the Bethe lattice it is exponential, both behaviors being particular cases of Eq. (19).

In general, for moderate to large U_i, the dynamics of the TDGA spectral gap [cf. Fig. 3(c)] is determined by both the fast double occupancy oscillations at frequency Ω_U (which are not resolved in the figure) and the slower oscillations of the Gorkov function at frequency Ω_J, which are revealed in the envelope of $\Delta(t)$. To summarize this part, we see that in the present regime the Gorkov function shows a BCS-like dynamics [17–19] while the gap has an additional high frequency which is not present in weak coupling time-dependent BCS theory. In Sec. V we show that both features also appear in the optical conductivity, even at weak coupling in the transient regime, which therefore in principle allows us to validate the present approach in pump probe experiments.

B. $|U_F| > |U_i|$ quench

1. Weak and moderate coupling

One way to characterize the weak coupling (BCS) limit of the dynamics is by comparing the spectral gap Δ_μ with the product of the interaction and the Gorkov function J^-. For small values of the interaction *and* small interaction quenches one should recover the BCS dynamics where the two quantities are related by $\Delta_\mu = |U|J^-$. We first check the range of validity of this expression at equilibrium in the inset panels of Figs. 4(a) and 4(b), where both sides of the equation are shown as a function of the interaction. We see that in this case this relation holds when both quantities become exponentially small, i.e., for small attractive interaction.

In order to study the crossover in the nonequilibrium case we show in Figs. 4(c) and 4(d) the dynamics of Δ_μ and $|U_F|J^-$ for interaction quenches from $U_i = -0.3$ to $U_F = -0.4$ and $U_F = -0.32$. It can be seen that dynamically at short times the difference between Δ_μ and $|U_F|J^-$ becomes important, even in a regime where the equilibrium computation shows

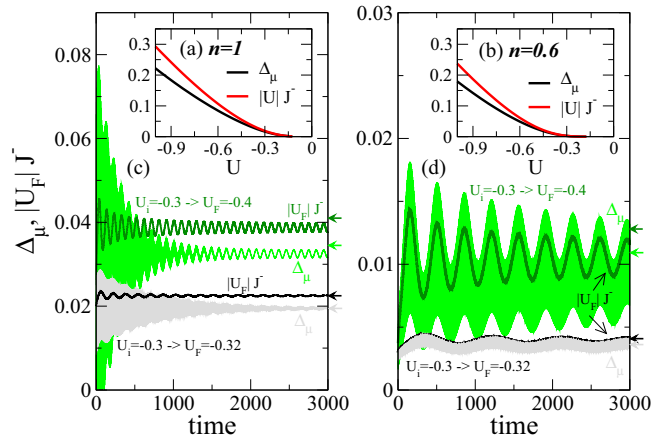

FIG. 4. Dynamics of the spectral gap Δ_μ and the Gorkov function J^- near the weak coupling regime. As a reference, the inset panels (a) and (b) compare the equilibrium spectral gap Δ_μ (black) with the equilibrium Gorkov function scaled by $|U|$ (red) for densities $n = 1$ (a) and $n = 0.6$ (b). Panels (c) and (d): Time dependence of Δ_μ (light green, gray) and $|U|J^-$ (dark green, black) for a U quench from $U_i = -0.3$ to $U_F = -0.4$ and $U_F = -0.32$ for densities $n = 1$ (c) and $n = 0.6$ (b). Results are for a two-dimensional square lattice. Arrows at the right axis mark the corresponding equilibrium values for $U = U_F$.

small or moderate differences. Indeed, Δ_μ shows again the fast dynamics due to the double occupancy fluctuations which are absent in $|U_F|J^-$. Comparing moderate ($U_F = -0.4$) and small ($U_F = -0.32$) quenches in Fig. 4 we see that the transient phase extends longer in time for smaller quenches but the associated oscillations of the gap decrease in amplitude with a concomitant decrease in the difference between Δ_μ and $|U_F|J^-$. In both cases the difference at short times is surprising given that the values of U_F are in a regime where at equilibrium there is little difference between the two quantities.

Away from half filling, the coupling of the gap to the double occupancy oscillations is significantly enhanced and the associated fast oscillations in Δ_μ appear with a much larger decay time (not shown, we find $t \approx 10\,000$ for $U_i = -0.3$, $U_F = -0.4$, and $n = 0.6$). However, similar to the half-filled case the crossover to the BCS dynamics occurs via a decrease of the width of these fast oscillations so that the envelope of Δ_μ approaches $|U_F|J^-$ in the limit of small interaction quenches (and small U_i). Eventually, a BCS-like dynamics is recovered in all cases at long times but important differences remain in a transient phase which also reflect in the optical conductivity, see Sec. V.

In BCS the Larmor precession frequency of pseudospins (corresponding to the phase velocity of the momentum resolved Gorkov function J_k^-) is determined by the z component of the pseudomagnetic field through a Bloch equation as in Eq. (14) [19,21]. Analogously, here we find that in the regime of Fig. 4 the phase velocity is found to obey $\omega_p = 2(q_\parallel \varepsilon_k - \mu)$ [cf. Eq. (15)].

We now discuss the long time averages of the various quantities, see Figs. 5 and 6. In the weak-coupling regime and for small quenches, the long-time average values of the Gorkov function [scaled by U_F, panels (b)] is slightly below but close to the equilibrium value (gray solid line) as in the

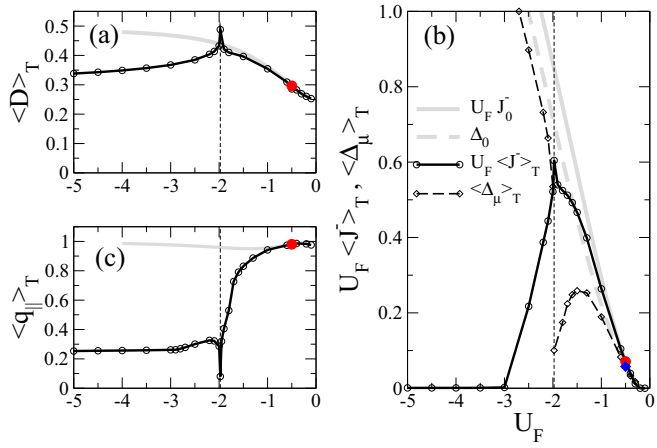

FIG. 5. Long-time averages of (a) double occupancy $\langle D\rangle_T$, (b) Gorkov function $\langle J\rangle_T$ scaled by U_F (circles) and $\langle\Delta_\mu\rangle_T$ (diamonds), (c) Gutzwiller renormalization factor $\langle q_\parallel\rangle_T$. for a quench from $U_i = -0.5$ to U_F in a half-filled square lattice. The full red circles correspond to the equilibrium values at U_i [in panel (b) full circle (blue diamond) are equilibrium values for $U_F J^-$ (Δ_0)]. The gray lines show the equilibrium value for $U = U_F$ and the vertical dotted line indicates the dynamical phase transition at U_c.

BCS case. It is interesting that the average gap $\langle\Delta_\mu\rangle_T$ is much more sensitive to a deviation from the weak coupling regime as compared to $U_F\langle J\rangle_T$, leading to a divergent behavior of both quantities as $|U_F|$ is increased.

For weak to moderate coupling also the long-time average of the double occupancy is close to the equilibrium value [Figs. 5(a) and 6(a)]. In this regime superconducting correlations weakly influence on the characteristic frequency of the double occupancy oscillations Ω_U. In the half-filled system a linear response analysis [31] yields $\Omega_U = 4|\varepsilon_0|\sqrt{q_0}$ where ε_0 denotes the kinetic energy (per site) of the noninteracting system and q_0 is the (equilibrium) Gutzwiller renormalization factor. Figure 8(a) (star symbol) reveals the reasonable agreement of this estimate with the result of the full calculation (triangles) for small quenches.

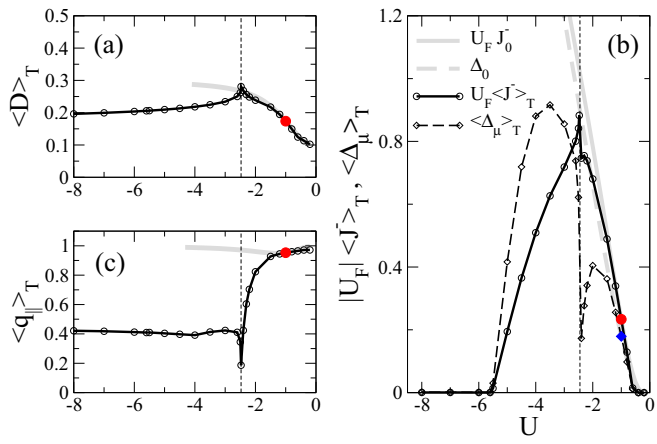

FIG. 6. Same as Fig. 5 but for concentration $n = 0.6$.

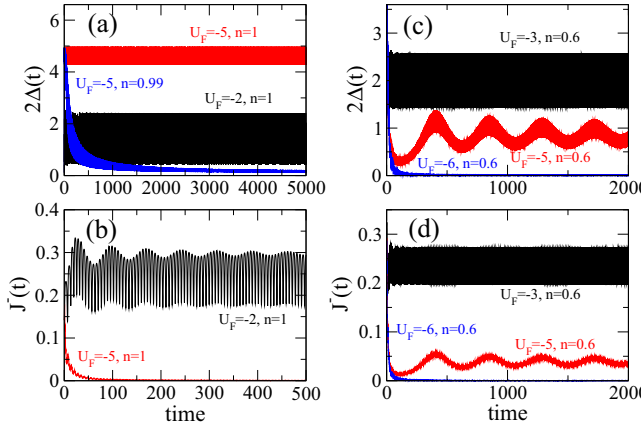

FIG. 7. Dynamics of the spectral gap $\Delta(t)$ [panels (a) and (c)] and the Gorkov function $J^-(t)$ [panels (b) and (d)] in the regime $|U_F| > |U_i|$ for $U_i = -0.5$, $n = 1$ [panels (a) and (b)] and $U_i = -1$, $n = 0.6$ [panels (c) and (d)].

2. *Strong coupling*

For large quenches $|U_F|/|U_i| \gg 1$ the BCS dynamics crosses over to a synchronized regime [17,19] characterized by phase locked Cooper pair states and an order parameter dynamics which oscillates nonharmonically between two extrema Δ_- and Δ_+. Remarkably, even in this regime the main frequency of the order parameter in the pure BCS dynamics is determined by the average spectral gap, i.e., it obeys Eq. (18). Although the proof is simple, we are not aware of it in the BCS literature, so we explicitly show it in Appendix B. The validity of the BCS dynamics requires that $|U_F|, |U_i| \ll 1$. The TDGA approximation allows us to relax that restriction and explore the intermediate and large coupling regime. As we will show below, for the present parameters and large $|U_F|$ the TDGA replaces the synchronized regime by a damped dynamics with zero final average gap and Gorkov function except exactly at half filling ($n = 1$).

Figure 7 illustrates the dynamics for $|U_F| > |U_i|$ near or at $n = 1$ (left column) and for $n = 0.6$ (right column). It is apparent from Figs. 7(a) and 7(c) that, as in the previous cases, the dynamics of $2\Delta(t)$ is dominated by the fast double occupancy oscillations which are not resolved on the scale of the plot and which give rise to the filled finite width in the time evolution. For the half-filled case [panel (a)] the average gap increases with $|U_F|$ (roughly $2\Delta \sim |U_F|$) while the amplitude of the oscillation decreases. The exactly half-filled case is special, in particular at strong coupling, as a small deviation changes dramatically the long-time behavior for $|U_F| \gg |U_i|$ as can be seen comparing the red line ($n = 1$) with the blue line ($n = 0.99$) in Fig. 7(a). While in the first case the gap oscillates around a finite value $\Delta_\mu \sim |U_F|$, the time evolution of the spectral gap in the second case starts from a similar initial value but then relaxes with a $1/\sqrt{t}$ behavior to zero. On the other hand, $\langle J^-\rangle_T$ [Fig. 7(b)] is strongly suppressed for large final interaction ($U_F = -5, -6$) so that the BCS relation $\langle\Delta_\mu\rangle_T = U_F\langle J^-\rangle_T$ analyzed in Sec. III B 1 is strongly violated here.

The transition from weak to strong $|U_F|$ is separated by a dynamical phase transition at a critical interaction U_c [32,33,39,40]. This is characterized by the dynamics of the

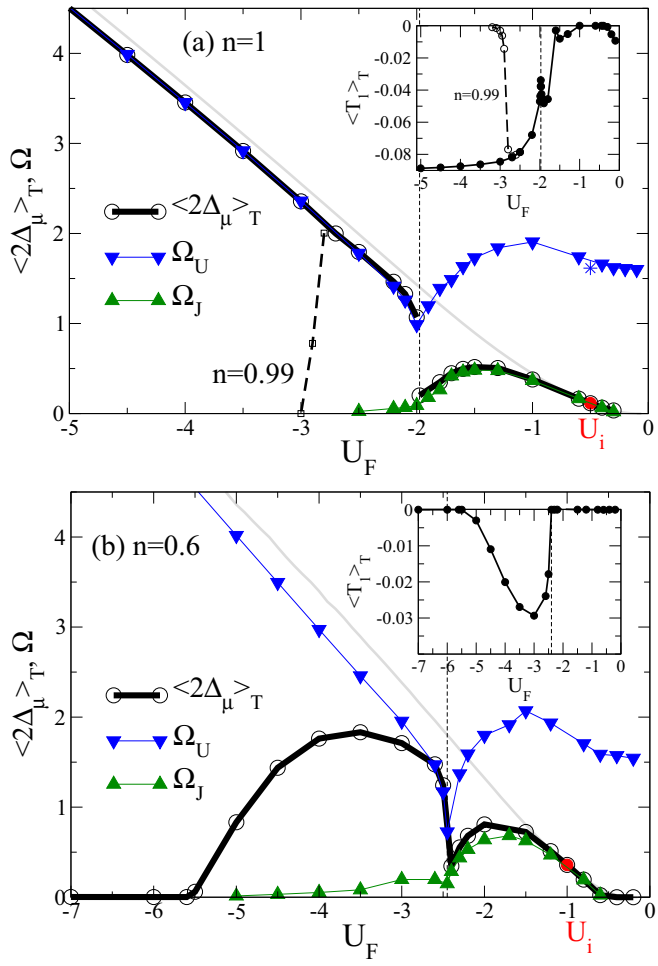

FIG. 8. Long-time averages of the spectral gap (black, circles) compared to the main frequencies Ω_U (triangles down, blue) and Ω_J (triangles up, green) in the dynamics for: (a) quench from $U_i = -0.5$ and $n = 1$, (b) and $U_i = -1$ and $n = 0.6$. The horizontal axis is the final U_F while the red dots indicate U_i. The dashed line in the inset of panel (a) shows T_1 for $n = 0.99$. The dashed line in the main panel shows the average of the spectral gap for $n = 0.99$. The insets report the long-time average of the anomalous kinetic energy T_1 (full line), cf. Eq. (3). The vertical dotted line indicates the dynamical phase transition at U_c. In panel (a) we also show results for $n = 0.99$ (dashed line) and the star symbol indicates the value of Ω_U from linear response [31] in the normal system.

phase η which changes from oscillating around zero to a precession around the unit circle. Figure 1 compares the density dependence of U_c for two initial U values, $U_i = -0.5$ and $U_i = -1$ with the Brinkman-Rice equilibrium transition. Clearly the typical scale of U for both transitions is the same.

Exactly at U_c the average Gutzwiller renormalization factor $q_\parallel$ approaches zero [cf. Appendix C and Figs. 5(c) and 6(c)], indicative of an insulating state. The transition reflects as a maximum in the time averaged double occupancy [cf. Figs. 5(a) and 6(a)] reaching the value corresponding to full localization $D = n/2$.

Examining the dynamics it has been shown [32,33] that approaching U_c, the period in which Gutzwiller renormalization factors tend to zero, logarithmically diverges. The finite values of $q_\parallel$ shown in the figures are due to the slow (logarithmic) convergence of the averages at U_c.

As already mentioned in the previous subsection, the long-time average of the Gorkov function [circles, panel (b) of Figs. 5 and 6] initially increases with $|U_F|$ and stays slightly below the equilibrium value for $U \equiv U_F$ (gray solid line). In the same panels we also report the long-time average of the spectral gap $\langle \Delta_\mu \rangle_T$ (diamonds). It also first follows a BCS-like behavior upon increasing $|U_F|$, slightly below the equilibrium value (gray dashed line), but then goes through a maximum and approaches a minimum at $U_F = U_c$. For $n = 1 \langle \Delta_\mu \rangle_T$ shows a discontinuity at $U_F = U_c$ and increases for $U_F > U_c$ whereas away from half filling a cusp appears at $U_F = U_c$ and $\langle \Delta_\mu \rangle_T$ vanishes together with the Gorkov function at large U_F. This demonstrates that the BCS relation between $\langle \Delta \rangle_T$ and $\langle J^- \rangle_T$ is strongly violated as soon as U_F deviates from a strict weak coupling regime.

The maximum of the Gorkov function at U_c might seem paradoxical at first sight as it implies that the underling BCS state still has a well-defined phase and pairing amplitude. In reality the pairs are fully localized so notwithstanding the phase is well defined, this state is extremely fragile, i.e., the cost to scramble it is very low and the kinetic energy of the pairs is completely suppressed. More precisely, we will in Sec. V see that the phase stiffness ρ_s tends to vanish at U_c.

For larger values of $|U_F|$ the Gorkov function diminishes and finally vanishes. This suppression of the Gorkov function for large quenches is opposite to what is obtained within the time-dependent BCS approach but agrees with nonequilibrium studies within DMFT [47] in the context of quenched antiferromagnetism. For the half-filled system this vanishing of the Gorkov function implies the vanishing of local superconducting correlations. However, anisotropic superconducting s-wave correlations still persist in this regime as can be seen from the insets to Fig. 8 where we report the long-time average of anomalous kinetic energy correlations T_1, which contributes to the total energy in the TDGA, cf. Eq. (3). For our two-dimensional system with $\varepsilon_k = -2t[\cos(k_x) + \cos(k_y)]$, Fourier transformation of Eq. (4) yields a contribution to the energy which only depends on a symmetric combination of SC correlations between nearest neighbors, i.e., extended s-wave symmetry, while the bare (i.e., local) s-wave correlations vanish in the regime of large U_F at half filling. Moving slightly away from half filling (dashed line in the inset to Fig. 8) the intersite SC correlations vanish together with the Gorkov function as shown in Fig. 7(a). For $|U_F| \gtrsim 3$ the half-filled system is characterized by finite intersite but vanishing local SC correlations and the persistence of an average spectral gap which is of the same energy scale as the local on-site attraction. Away from half filling extended and local s-wave correlations vanish together with the spectral gap at large $|U_F|$ [cf. Fig. 6(b) and inset to Fig. 8(b)]. Therefore in all cases we never observe a real "pseudogap state" because the region of finite spectral gap coincides with the region of SC correlations. In Sec. IV we will analyze this in more detail and show how the double occupancy fluctuations drive the fermions and with increasing strength suppress the average Gorkov function.

Figure 8 compares the characteristic frequencies of the dynamics Ω_U (double occupancy, blue triangles) and Ω_J

(Gorkov function, green triangles). Upon increasing $|U_F|$, starting from $|U_i|$, Ω_J has a dome shape, somehow similar to the Gorkov function $\langle J^- \rangle_T$ [Fig. 5(b), 6(b)], until both quantities vanish. Instead, Ω_U remains large and of the order of the bandwidth until for $|U_F| > |U_c|$ it increases linearly with $|U_F|$ with a cusp singularity at U_c. In the same figure we also show the long time average $\langle 2\Delta_\mu \rangle_T$ (black lines and circles). For $|U_F| < |U_c|$, Ω_J follows $\langle 2\Delta \rangle_T$ (similar to the BCS case) but then at U_c the singular behavior in $\langle 2\Delta \rangle_T$ arises and Ω_J decouples from the gap. For $|U_F| > |U_c|$ and half filling the roles are interchanged and the gap follows Ω_U. Note that $\langle 2\Delta \rangle_T = \Omega_U$ holds even in the regime where $\langle J^- \rangle_T = 0$. Away from half filling this behavior persists close to U_c but then Ω_U keeps increasing as $|U_F|$ thus decoupling from the gap which is instead suppressed for large $|U_F|$.

The gray lines in Fig. 8 show the $T = 0$ equilibrium value of the gap as a function of $U = U_F$ showing how the smooth crossover is replaced by the dynamical transition in the out-of-equilibrium situation. Although for large quenches (corresponding to large injection of energy into the system) the long-time average of the spectral gap vanishes for $n \neq 1$ there remains a visible signature of the pair breaking energy via the Ω_U frequency which is slightly below the BCS equilibrium spectral gap.

In BCS it has been shown that the average gap value at long times of the nonthermal BCS dynamics is near the value the system would have for a closed system at thermodynamic equilibrium [19]. Thus, for large quenches in which the interaction is *reduced* the average gap becomes zero corresponding to an effective temperature larger than the critical temperature. This breaks down for a large quench in which the interaction is *increased* since in that case the synchronized regime is found instead of the gapless state. Thus in BCS, the same amount of injected energy has very different outcomes depending on if the interaction is reduced or increased. In the TDGA the situation is more symmetric as large quenches in both directions lead to a suppressed Gorkov function.

IV. FREQUENCY MIXING AND SELF-SUSTAINED RABI OSCILLATIONS

In BCS the spectral gap after a quench oscillates with its natural frequency Ω_J. As it is clear from Figs. 3, 4, and 7 the Gutzwiller dynamics is more complex. Besides the frequency Ω_J the spectral gap responds to the fast oscillations of the double occupancy with frequency Ω_U. Figure 9(a) shows the Fourier transform of the spectral gap. We see indeed that Ω_J and Ω_U emerge as the prevailing frequencies, but due to the intrinsic nonlinearities of the dynamics other frequencies emerge.

From the equations of motion, we notice that the double occupancy oscillations are seen by the pseudospin degrees of freedom as "external" periodic drives. In fact, the modulation of the bandwidth via $q_\parallel(t)$ [cf. Eq. (15)] adds a time dependence to the effective magnetic field along the z direction, $b_k^z = q_\parallel(t)\varepsilon_k$ which we write as $b_k^z = b_k^{z,0} + \delta b_k^z(t)$. Here $b_k^{z,0} = \langle q_\parallel(t) \rangle_T \varepsilon_k$ is determined by the temporal average of the renormalization factor and we approximate the time dependent part as $\delta b_k^z(t) \approx \gamma \varepsilon_k \cos(\Omega_D)$ where Ω_D is the frequency of the drive. In linear response, the spectral gap responds to

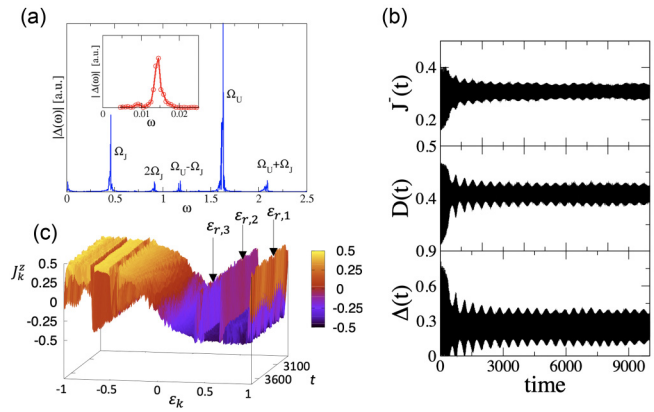

FIG. 9. (a) Fourier spectrum of $\Delta(\omega)$. The inset details the low energy part with the Rabi excitation. Quench $U_i = -0.5 \to U_F = -1.6$ in the half-filled 2D system. (b) From top to bottom: Gorkov function, double occupancy, and spectral gap. (c) Energy and time dependence of the pseudospin J_k^z showing population inversion at energies $\varepsilon_{r,i}$.

fluctuations of the double occupancy, δD at the frequency of the driving according to,

$$\delta\Delta_\mu(t) = \chi_{\Delta n}\delta b_k^z(t), \tag{20}$$

where $\chi_{\Delta n}$ is a gap-charge susceptibility (see Ref. [52] for an analogous treatment in the BCS problem). In addition, there is an explicit dependence of Δ_μ on D through equations Eqs. (A1)–(A4) and (A8). So overall we can write,

$$\delta\Delta_\mu(t) = \left(\chi_{\Delta n}\frac{\partial b_k^z}{\partial D} + \frac{\partial \Delta_\mu}{\partial D}\right)\delta D(t) \tag{21}$$

which explains the appearance of the Ω_U peak in Fig. 9(a). Extending the expansion to second order in the $\delta D(t)$ and $\delta J^\pm(t)$ fluctuations, similarly explains the $2\Omega_J$ and the $\Omega_U \pm \Omega_J$ peaks. In fact, Raman like matrix elements $\partial\chi_{\Delta n}/\partial J^\pm$ produce Stokes and anti-Stokes responses at $\Omega_U \pm \Omega_J$ where Ω_U plays the role of a "photon." Furthermore, the second harmonic frequency $2\Omega_J$ is generated from $\delta J^+(t)\delta J^-(t)$ terms which are already present in $\delta b_k^z(t)$ through Eq. (A1).

Besides these linear, nonlinear, and Raman-like processes another slower characteristic frequency appears when one examines the dynamics in very long time windows. For example, for quenches $|U_i| < |U_F| < |U_c|$ in the regime where $\langle J^- \rangle_T$ and Ω_J are maximum ($U_F \sim -1.6$ in Fig. 5) one observes very slow oscillations in the envelope of all dynamical quantities as shown in Fig. 9(b) for the half-filled system and a quench $U_i = -0.5 \to U_F = -1.6$. This new frequency is not directly related to the previous ones. Indeed, the Fourier transform of this oscillation yields $\Omega_R \approx 0.014$ [inset of Fig. 9(a)] whereas the frequencies of Gorkov function and double occupancy are $\Omega_J = 0.46$, $\Omega_U = 1.63$ [main panel (a)]. The slow frequency seems to decrease upon approaching U_c.

In order to shed some light on this excitation we show in Fig. 9(b) the pseudospin dynamics of J_k^z as a function of the energy ε_k. One observes population inversion at energies $\varepsilon_{r,1} \approx 0.98$, $\varepsilon_{r,2} \approx 0.68$, and $\varepsilon_{r,3} \approx 0.46$. Such population inversion in the momentum distribution function (J_k^z) is characteristic of collective Rabi oscillations occurring in a

superconductor subject to a periodic drive [52,53]. In the case of a pure BCS dynamics as considered in Ref. [52] and for a band width drive, collective Rabi oscillations are due to states at "resonant" energies

$$\bar{q}\varepsilon_k \equiv \bar{q}\varepsilon_{r,i} = \frac{1}{2}\sqrt{\Omega_D^2 - (2\Delta)^2}\,, \tag{22}$$

where the average renormalization factor $\bar{q} = 1$ in BCS. The corresponding pseudospin will then perform a precession around $b_k^\perp$, which is the field component of $\mathbf{b}_k(t)$ perpendicular to the static (or time-averaged) field $\mathbf{b}_k^0(t)$ [52]. Analogous to magnetic resonance dynamics [60] the precession ('Rabi') frequency would then be given by

$$\Omega_R = \frac{1}{2}b_k^\perp = \gamma\Delta\sqrt{1-(2\Delta/\Omega_D)^2}\,. \tag{23}$$

In the present time-dependent Gutzwiller dynamics, drives are generated internally as discussed above. Based on these arguments the energies $\varepsilon_{r,i}$ at which population inversion is expected can be obtained by replacing in Eq. (22) Ω_D by combinations of Ω_U and Ω_J and also including the average band width renormalization $\bar{q} = \langle q_\parallel\rangle_T$,

$$\varepsilon_{r,1} = \frac{1}{2\bar{q}}\sqrt{\left(\Omega_D^{(1)}\right)^2 - (2\Delta)^2} \approx 0.98 \quad \text{for} \quad \Omega_D^{(1)} = \Omega_U$$

$$\varepsilon_{r,2} = \frac{1}{2\bar{q}}\sqrt{\left(\Omega_D^{(2)}\right)^2 - (2\Delta)^2} \approx 0.67 \quad \text{for} \quad \Omega_D^{(2)} = \Omega_U - \Omega_J$$

$$\varepsilon_{r,3} = \frac{1}{2\bar{q}}\sqrt{\left(\Omega_D^{(3)}\right)^2 - (2\Delta)^2} \approx 0.49 \quad \text{for} \quad \Omega_D^{(3)} = 2\Omega_J$$

where for the considered quench we have $\bar{q} \approx 0.79$ and $2\Delta \approx 0.49 \approx \Omega_J$. The above theoretical estimates are in excellent agreement with the frequencies at which population inversion is seen in Fig. 9(c) giving support to our hypothesis that Ω_U and Ω_J are acting as "external" driving frequencies. Notice that the combination $\Omega_U + \Omega_J$ would correspond to a drive outside the available energy spectrum and therefore does not produce a resonance for the present parameters.

Based on this knowledge we can now ask the question of how these drives are related to the slow Rabi oscillation visible in Fig. 9. Generalizing Eq. (23) to include the bandwidth renormalization and taking $\gamma \approx 0.05$ as obtained from the width of the renormalization factor dynamics $q_\parallel(t)$ one obtains

$$\Omega_R^{(1,2,3)} = \Delta\frac{\gamma}{\bar{q}}\sqrt{1-\left(2\Delta/\Omega_D^{(1,2,3)}\right)^2} \approx 0.015, 0.014, 0.013\,.$$

The low energy Fourier transform of $\Delta(\omega)$ in the inset of Fig. 9(a) consists of an excitation centered at $\omega_R \approx 0.014$ with a broadening which comprises the above frequencies which again supports the consistency of our analysis.

V. OPTICAL CONDUCTIVITY

We finally analyze how the characteristic frequencies, discussed in the previous section, are visible in the optical conductivity. In the nonequilibrium state we evaluate this quantity from the current response

$$\mathbf{j}(t) = \int_{t_0}^{t_0+T} dt'\sigma(t,t')\mathbf{E}(t') \tag{24}$$

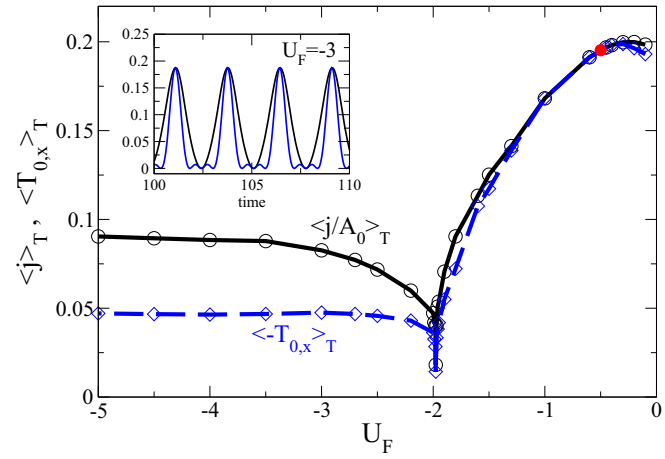

FIG. 10. Main panel: Drude weight $\mathcal{D} = j(0)/A_0$ (black, solid) compared to the regular kinetic energy (blue, dashed) as a function of the quenched interaction U_F for a half-filled square lattice. The red point indicated the equilibrium value U_i. Inset: Time dependence of both quantities for $U_F = -3$.

to a delta-like electric field $\mathbf{E}(t') = \mathbf{A}_0\delta(t'-t_1)$ which is applied within the interval $t_0 < t_1 < t_0 + T$ in which the current is measured. Then the optical conductivity is obtained from the Fourier transformed of Eq. (24) as [61]

$$\mathbf{j}(\omega) = \mathbf{A}_0 e^{i\omega t_1}\sigma(\omega, t_1)\,. \tag{25}$$

Within our model the delta-shaped electric field is coupled to the system by a steplike vector potential $\mathbf{A}(t) = \mathbf{A}_0\Theta(t - t_1)$ via the standard Peierls substitution say along the x direction. This induces a shift of momentum $k_x \to k_x + A_x$ and the current is evaluated from $j(t) = \delta E^{\mathrm{GA}}/\delta A_x$. Then the Fourier transform of $j(t)$ is performed for times $t_1 \lesssim t \lesssim t_1 + t_{\max}$.

In equilibrium BCS theory and for a homogeneous single band system only a diamagnetic current is induced by A_x [62] and one finds that both charge and phase stiffness are the same and given by the kinetic energy. The same is valid in the equilibrium TDGA (which can be shown along similar lines as in Ref. [62]) where in equilibrium only the normal contribution to the kinetic energy T_0 [cf. Eq. (3)] is finite.

In nonequilibrium and within standard time-dependent BCS theory the linear coupling of a vector potential still leads to a purely time-dependent diamagnetic current which therefore is equivalent to the time-dependent kinetic energy. The charge stiffness (Drude weight) $\mathcal{D}$, defined as the $\omega = 0$ component of this current, is then just the time averaged kinetic energy.

In contrast, the Peierls substitution in the TDGA also influences on the pairing term $\sim q_\perp\varepsilon_k$ [cf. Eqs. (3) and (4) and Appendix A] which generates an additional pairing component $\sim T_1$ to the current, which is significant in particular at large quenches U_F and close to half filling as can be seen from the inset to Fig. 8.

The main panel of Fig. 10 compares $\mathcal{D}$ with the regular kinetic energy T_0 [cf. Eq. (4)] along x as function of the quenched interaction U_F. For $U_F \approx U_i$ both quantities coincide since in this limit the oscillation of the double occupancy phase vanishes and therefore also $q_\perp \to 0$. Differences occur

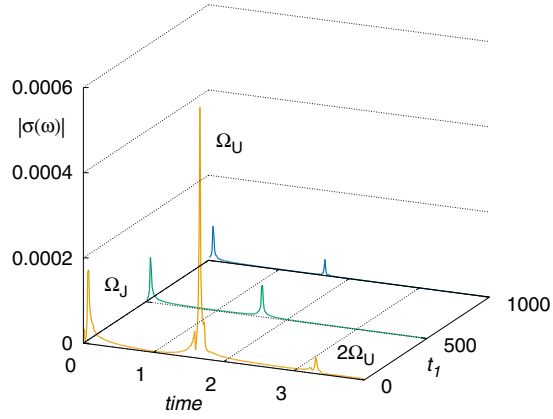

FIG. 11. Optical conductivity (magnitude) $|\sigma(\omega, t_1)|$ for $n = 1$ and a quench $U_i = -0.3 \to U_F = -0.4$. The Fourier transform is obtained from the time evolution between t_1 and $t_1 + t_{\max}$ with $t_{\max} = 500$.

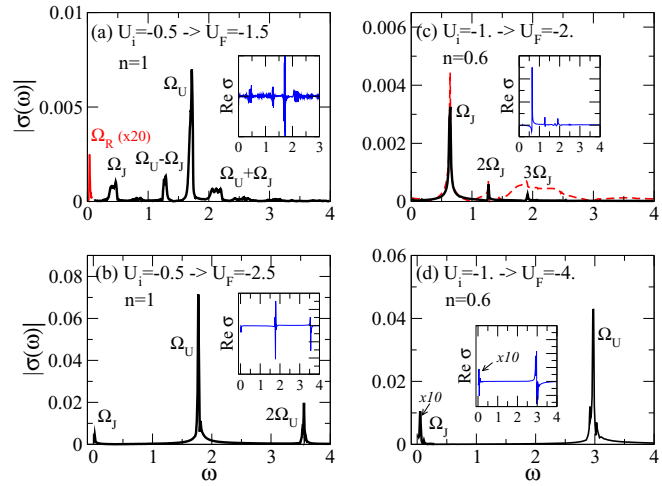

FIG. 12. Optical conductivity $\sigma(\omega, t_1 = 50)$ for $n = 1$ [(a),(b)] and $n = 0.6$ [(c),(d)] and different quenches as indicated in the panels. Main panels show the magnitude $|\sigma(\omega, t_1)|$ whereas insets report the real part. Panel (c) also reports $|\sigma(\omega, t_1)|$ for $t_1 = 0$ (red dashed) which contains the Ω_U excitations in the transient regime. In panel (a) the Fourier transform has been performed for times up to $t_{\max} = 2500$ whereas in panels (b)–(d) $t_{\max} = 500$.

for large quenches and close to half filling, in particular for $|U_F| > |U_c|$, where the normal component of the kinetic energy underestimates the Drude weight by almost a factor of two for the present parameters. Notice that since this is an out of equilibrium situation the Drude weight is not constrained by the f-sum rule to be smaller than the kinetic energy and indeed this condition is strongly violated.

The phase stiffness is given by a similar computation as the Drude weight but the limit $\omega \to 0$ has to be taken before the limit $q \to 0$ for a momentum and frequency dependent vector potential $A(q, \omega)$. In equilibrium, for a gapped system at $T = 0$ the two limits coincide as the paramagnetic contribution to the current is zero [62]. Being out of equilibrium we will have additional absorption process due to excited quasiparticles but we still expect that the Drude weight as computed above provides an upper bound for the superfluid stiffness. Thus, the strong suppression of the Drude weight at U_C is indicative of a system which is very fragile to phase fluctuations.

In equilibrium linear response, both BCS and TDGA do not display an absorption at $\omega > 0$ for a homogeneous SC. In fact, a photon with $q = 0$ couples neither to the quasiparticle nor to the amplitude excitation at $\omega = 2\Delta$. Also double occupancy fluctuations are invisible in the linear response TDGA optical conductivity because these only couple to charge fluctuations, and since the charge-current vertex vanishes for $q \to 0$. the excitation at Ω_U is decoupled from the current. The situation is different in nonequilibrium where the investigation of associated optical properties is an active field in the context of 'Higgs spectroscopy,' see, e.g., Refs. [63,64] and references therein. Figure 11 reports the magnitude of the optical conductivity $|\sigma(\omega)|$ in the weak coupling regime for a quench $U_i = 0.3 \to U_F \to -0.4$ [cf. Fig. 4] and within different time intervals $t_1 \leqslant t \leqslant t_1 + t_{\max}$ of the dynamics. Due to the nonequilibrium situation one now observes the amplitude mode at $\Omega_J \approx 0.065$ slightly below the equilibrium gap $2\Delta = 0.072$ for $U = -0.4$. In addition, the double occupancy oscillations at Ω_U become visible in the optical conductivity, where in the early transient phase ($t_1 = 1$) even the second harmonic at $2\Omega_U$ is admixed. Moving the time window for the Fourier transformation to later times, the Ω_U peak rapidly looses intensity whereas the amplitude ('Higgs') mode is only slightly decreased with respect to the early transient phase. Thus, in the long-time limit $t_1 \to \infty$ and weak coupling we recover the nonequilibrium BCS result with only the Higgs-mode visible in $\sigma(\omega)$.

In case of stronger coupling and larger quenches Fig. 12 reports $\sigma(\omega, t_1)$ and the corresponding density of states (DOS) has been evaluated in Appendix D. For a better visualization of the involved frequencies we show in the main panel the magnitude $|\sigma(\omega, t_1)|$ whereas the insets display the real part $\sigma'(\omega, t_1)$ with $t_1 = 50$. Again both frequencies Ω_J and Ω_U are visible in $\sigma(\omega, t_1)$ except for panel c) where the Ω_U oscillations are already damped for $t < t_1 = 50$ and are only visible as a broad feature if the field is switched on already at $t_1 = 0$ (red dashed).

A further feature is the coupling of the order parameter to the double occupancy dynamics, as discussed in the previous section, which is especially apparent in panel (a) of Fig. 12 where Ω_U has two side peaks at $\Omega_U \pm \Omega_J$ as discussed in the previous section. This coupling is also present in panels (b) and (d) but hardly visible on the scale of the plot due to the smallness of Ω_J. In panel (a) we have performed the Fourier transform up to large times $t_{\max} = 2500$ which includes several Rabi periodicities. The Rabi oscillation is visible in $\sigma(\omega)$ though the intensity is much smaller than those of the main excitations at Ω_J and Ω_U. Finally, it should be noted that for large quenches higher harmonics of Ω_U appear in the conductivity (cf. panel c).

We conclude that the TDGA adds the doublon scale Ω_U to the nonequilibrium optical conductivity in contrast to the analogous result in BCS theory where the spectra are only characterized by the Ω_J feature. Even in the weak coupling limit (cf. Figs. 4 and 11) the Ω_U excitation can be seen in the

transient phase which in principle allows to inspect the BCS vs TDGA dynamics in a pump probe experiment.

VI. CONCLUSIONS

We have analyzed the dynamics of out-of equilibrium superconductivity within the time-dependent Gutzwiller approximation. As shown previously [39,40] this approach correctly reproduces certain aspects of nonequilibrium DMFT [47–49] as the trapping in nonthermal states and the appearance of two energy scales in the transient dynamics.

In particular, DMFT reveals a sharp crossover in the dynamics of the Hubbard model upon quenching the noninteracting system to a finite interaction U [46]. In the weak coupling regime, below a critical interaction U_c, the double occupancy $D(t)$ relaxes to the almost thermalized value whereas for strong coupling $D(t)$ recovers and oscillates with frequency $\sim U$. The TDGA captures this feature as a 'dynamical generalization' of the Brinkman-Rice transition [57], keeping in mind that for the negative U model the latter occurs at every density. The state reached at $U_F = U_c$ is very peculiar, it is characterized by zero kinetic energy and fully developed composite bosons. Interestingly, this is reminiscent of a Brinkman-Rice insulator but made of bosons instead of fermions.

Two main frequencies, Ω_U and Ω_J, determine the dynamical quantities within the TDGA which for small quenches are related to the double occupancy and SC pair correlation dynamics. In DMFT [47,48] analogous frequencies have been determined for the dynamics of double occupancy and antiferromagnetic order parameter in the repulsive Hubbard model, which in case of half filling can be mapped onto the attractive model studied in the present paper.

At weak coupling a BCS dynamics is recovered at long times with Ω_J locked to the asymptotic average gap. However the TDGA transient has some important differences with BCS for not very large couplings and quenches which are visible in the optical conductivity.

In general, both from the study of average quantities as the spectral gap or dynamical quantities like the optical conductivity, we find that the out of equilibrium dynamics converges much more slowly to the weak coupling regime than equilibrium quantities. For example, while the equilibrium GA gap is close to BCS expectations in weak and moderate coupling, the transient TDGA dynamics differs considerably from BCS. This suggests that nonlinear probes will be much more sensitive to strong coupling effects than linear probes, which can serve ultimately to characterize more accurately the coupling of a given condensate.

We have found that the dynamical phase transition at $|U_c|$ is also associated with a decoupling of the lowest frequency Ω_J from the long-time average of the gap, in sharp contradiction with a BCS-like dynamics. The high frequency Ω_U also decouples from the gap except for a region $|U_F| > |U_c|$ which depends on the filling. At half filling Ω_U remains locked to the average spectral gap for increasing quenches $|U_F|$, even when the local pair correlations are already suppressed. We have shown that this regime of large spectral gap ($\sim|U_F|$) and zero local pair correlations is instead characterized by intersite SC correlations (extended s-wave symmetry) which also influence on the Drude weight. It would be interesting to see whether such crossover from local to extended s-wave superconducting correlations is also obtained in exact approaches in small systems or infinite dimensions.

The TDGA can be viewed as a driven BCS model where the drive acts on the bandwidth via the time dependence of the Gutzwiller renormalization factors. In an out-of equilibrium situation we have shown that the characteristic drive frequency is not only due to the double occupancy dynamics but can be a linear combination of the basic frequencies Ω_U and Ω_J. This yields a consistent explanation for the structure of low energy Rabi oscillations which can be observed in all dynamical quantities in certain parameter regimes where the resonant condition can be fulfilled. Moreover, since for a bandwidth driven BCS model the increase of the drive amplitude results in a suppression of the Gorkov function, it is most likely that the same mechanism is also responsible in the TDGA for the vanishing of J^- at large interaction quenches.

The TDGA does not include thermalization mechanisms so that in the long-time limit integrated quantities stay either oscillating or decay due to dephasing, cf. Fig. 7, whereas in an exact treatment one expects damping on a time scale τ_{th}. The open question therefore remains if real systems can be tuned towards a regime where τ_{th} is significantly larger than the Rabi periodicity which would allow the observation of the latter by nonequilibrium spectroscopic methods.

The protocol studied here can be realized in ultracold fermionic systems. For example, in Refs. [1,2] the fermion system is initially prepared on the BCS side of the Feshbach resonance and then, by a rapid lowering of the magnetic field, the gas is put far in the preformed pair regime. This corresponds to a sudden injection of energy in the system at $t = 0$. Such sudden change of interaction cannot be easily done in the solid state. However, one can inject some equivalent amount of energy in a pump-probe experiment. We have shown that depending on the coupling regime of the system, different features appear in probes as the optical conductivity. Therefore, at least in principle, a spectroscopic out of equilibrium experiment can give access to the relevant coupling parameters of the system.

ACKNOWLEDGMENTS

G.S. acknowledges financial support from the Deutsche Forschungsgemeinschaft. J.L. acknowledges insightful discussions with H.P. Ojeda-Collado, C.A. Balseiro, and G. Usaj on collective Rabi modes and financial support from Italian MAECI through bilateral project AR17MO7, from Italian MIUR through Project No. PRIN 2017Z8TS5B, and from Regione Lazio (L. R. 13/08) through project SIMAP.

APPENDIX A

The renormalization factors in Eq. (3) are given by

$$q_{\parallel} = Q_+^2 + \frac{J_z^2 - J^+J^-}{J^2} Q_-^2 \tag{A1}$$

$$q_{\perp} = 2iQ_- \frac{J^-}{J}\left[Q_+ - iQ_- \frac{J^z}{J}\right] \tag{A2}$$

with

$$Q_+ = \sqrt{\frac{\frac{1}{2} - D + J_z}{\frac{1}{4} - J^2}}\left[\sqrt{D - J_z - J} + \sqrt{D - J_z + J}\cos\eta\right]$$
$$Q_- = \sqrt{\frac{\frac{1}{2} - D + J_z}{\frac{1}{4} - J^2}}\sqrt{D - J_z + J}\sin\eta. \quad \text{(A3)}$$

Then the matrix elements become

$$H_{11}(k) = q_\parallel \varepsilon_k - \mu + \frac{U}{2}\left(1 - \frac{J^z}{J}\right) + \frac{\partial q_\parallel}{\partial J^z}\frac{1}{2N}\sum_{k'}\varepsilon_{k'}[R_{11}(k') - R_{22}(k') + 1] + \frac{1}{2N}\sum_{k'}\varepsilon_{k'}\left[\frac{\partial q_\perp}{\partial J^z}R_{12}(k') + \frac{\partial q_\perp^*}{\partial J^z}R_{21}(k')\right] \quad \text{(A4)}$$

$$H_{12}(k) = q_\perp^* \varepsilon_k - \frac{U}{2}\frac{J^+}{J} + \frac{\partial q_\parallel}{\partial J^-}\frac{1}{N}\sum_{k'}\varepsilon_{k'}[R_{11}(k') - R_{22}(k') + 1] + \frac{1}{N}\sum_{k'}\varepsilon_{k'}\left[\frac{\partial q_\perp}{\partial J^-}R_{12}(k') + \frac{\partial q_\perp^*}{\partial J^-}R_{21}(k')\right] \quad \text{(A5)}$$

$$H_{21}(k) = q_\perp \varepsilon_k - \frac{U}{2}\frac{J^-}{J} + \frac{\partial q_\parallel}{\partial J^+}\frac{1}{N}\sum_{k'}\varepsilon_{k'}[R_{11}(k') - R_{22}(k') + 1] + \frac{1}{N}\sum_{k'}\varepsilon_{k'}\left[\frac{\partial q_\perp}{\partial J^+}R_{12}(k') + \frac{\partial q_\perp^*}{\partial J^+}R_{21}(k')\right] \quad \text{(A6)}$$

$$H_{22}(k) = H_{11}(k). \quad \text{(A7)}$$

The spectral gap in Eq. (16) is defined as $\Delta_k = H_{12}^{\mathrm{GA}}(k) = \Delta_\mu + \Delta'_k$ with

$$\Delta_\mu \equiv \mu\frac{q_\perp^*}{q_\parallel} - \frac{U}{2}\frac{J^+}{J} + \frac{\partial q_\parallel}{\partial J^-}\frac{1}{N}\sum_{k}\varepsilon_{k}[R_{11}(k) - R_{22}(k) + 1] + \frac{1}{N}\sum_{k}\varepsilon_{k}\left[\frac{\partial q_\perp}{\partial J^-}R_{12}(k) + \frac{\partial q_\perp^*}{\partial J^-}R_{21}(k)\right], \quad \text{(A8)}$$

$$\Delta'_k \equiv \frac{q_\perp^*}{q_\parallel}(q_\parallel \varepsilon_k - \mu). \quad \text{(A9)}$$

APPENDIX B

Consider the synchronized regime where the self-consistent BCS dynamics is governed by the equation [17]

$$\dot{\Delta}^2 + (\Delta^2 - \Delta_-^2)(\Delta^2 - \Delta_+^2) = 0 \quad \text{(B1)}$$

and shows soliton solutions of the order parameter oscillating between $\Delta_- \leqslant \Delta(t) \leqslant \Delta_+$. The oscillation period is then

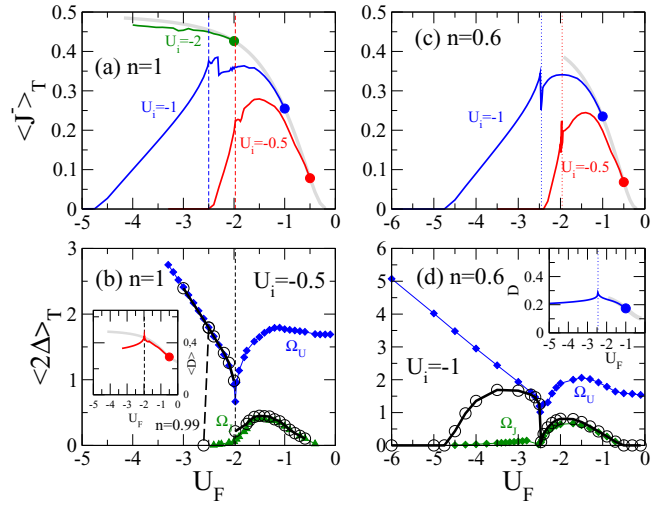

FIG. 13. Long-time averages of the Gorkov function [(a),(c)] and spectral gap [(b),(d)] for the Bethe lattice with infinite coordination number and concentrations $n = 1$ [(a),(b)] and $n = 0.6$ [(c),(d)]. Panels (b) and (d) also report the frequencies Ω_U, Ω_J and the insets show the long time average of the double occupancy.

determined from

$$T = 2\int_{T_-}^{T_+} dt = \int_{\Delta_-}^{\Delta_+}\frac{d\Delta}{\dot{\Delta}}. \quad \text{(B2)}$$

Similarly, the time-averaged order parameter is obtained from

$$\langle\Delta\rangle_T = \frac{2}{T}\int_{\Delta_-}^{\Delta_+} d\Delta\,\frac{\Delta}{\dot{\Delta}} \quad \text{(B3)}$$

so that

$$\langle\Delta\rangle_T = \frac{\omega}{\pi}\int_{\Delta_-}^{\Delta_+} d\Delta\,\frac{\Delta}{\sqrt{(\Delta^2 - \Delta_-^2)(\Delta_+^2 - \Delta^2)}} = \frac{\omega}{2} \quad \text{(B4)}$$

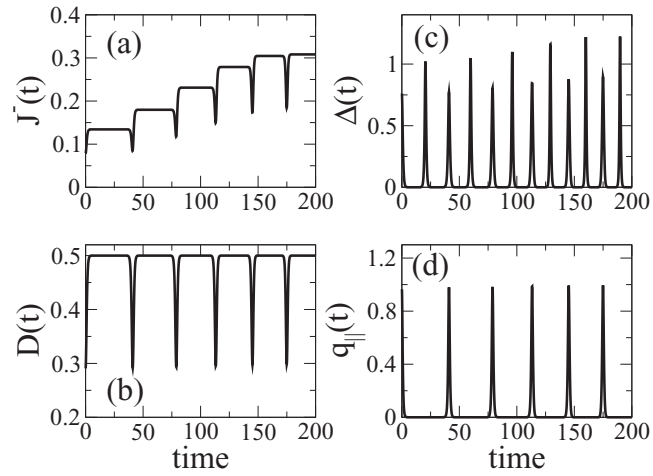

FIG. 14. Dynamics of the Gorkov function (a), double occupancy (b), hopping renormalization $q_\parallel$ (c), and spectral gap (d) in close vicinity to U_c. Results are obtained on a Bethe lattice with infinite coordination number and concentration $n = 1$.

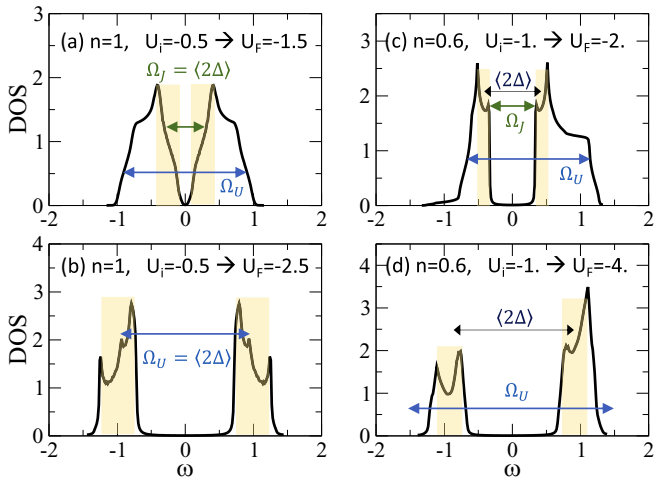

FIG. 15. Long-time averages of the DOS evaluated from Eq. (D1) for $n = 1$ [(a),(b)] and $n = 0.6$ [(c),(d)] and different quenches as indicated in the panels. Also shown are the characteristic frequencies (where sizable) Ω_J, Ω_U, cf. Figs. 5 and 6. The yellow shaded areas indicate the variation of the spectral gap in the time evolution (cf. Fig. 7). Parameters for the evaluation of $\langle\rho(\omega)\rangle_T$, cf. Eq. (D1): $t_0 = 500$, $T = 100$, $\eta = 5 \times 10^{-3}$.

where we have used Eq. (B1) and $\omega = 2\pi/T$ is the frequency of the oscillation. Thus also in the synchronized regime the main frequency ω of the BCS dynamics is determined by the time-averaged spectral gap $2\langle\Delta\rangle_T$.

APPENDIX C

Figure 13 reports the long-time averages of spectral gap [(a),(c)] and Gorkov function [(b),(d)] for a Bethe lattice with infinite coordination number. No qualitative changes occur with regard to the 2D case shown in Figs. 5 and 6.

The time dependence of Gorkov function $J^-(t)$, double occupancy $D(t)$, hopping renormalization $q_\parallel(t)$, and spectral gap $\Delta(t)$ close to the dynamical phase transition is shown in Fig. 14. The dynamics in this regime is characterized by a periodic soliton-like behavior with long localization time periods where $D(t)$ takes the Brinkman-Rice value ($D = 0.5$ for $n = 1$) and the hopping renormalization $q_\parallel$ vanishes. The time dependence of the phase $\eta(t)$ has a periodicity with twice the frequency of $D(t)$, $J^-(t)$, and $q_\parallel(t)$ which reflects also in the dynamics of the spectral gap $\Delta(t)$ [panel (c)].

APPENDIX D: DOS

In order to analyze the out-of equilibrium spectral properties we evaluate the density of states (DOS) obtained from the average

$$\langle\rho(\omega)\rangle_T = \frac{1}{T}\int_{t_0}^{t_0+T} dt\,\rho(\omega,t)$$

$$\rho(\omega,t) = Im\frac{1}{N\pi}\sum_k \frac{\omega + H_{11}^{\mathrm{GA}}(k)}{(\omega - i\eta)^2 - \left(H_{11}^{\mathrm{GA}}(k,t)\right)^2 - |\Delta_k(t)|^2}, \tag{D1}$$

where t_0 denotes a time scale after the initial transient dynamics and T is 'sufficiently longer' than the characteristic periodicities of the system. The elements of the Gutzwiller Hamiltonian H^{GA} are defined in Appendix A.

Figure 15 reports the DOS for concentrations $n = 1$ and $n = 0.6$ in case of different quenches $|U_F| > |U_i|$. Clearly the oscillation amplitude of $\Delta_k(t)$ has a large impact on the low energy structure of $\langle\rho(\omega)\rangle_T$. For example, at half filling and a quench $U_i = -0.5 \to U_F = -1.5$ the spectral gap oscillates between $0 \lesssim |\Delta(t)| \lesssim 0.5$ (not shown) which gives the impression of a 'd-wave'-shaped gap in the temporal average. Neither $\Omega_J = \langle 2\Delta\rangle_T$ nor Ω_U are apparent as peculiar feature in the averaged DOS. On the other, in case $U_i = -0.5 \to U_F = -2.5$ [panel (b)] the frequency $\Omega_U = \langle 2\Delta\rangle_T$ fits to the transition between two peaky structures in the DOS. For even larger values of $|U_F|$ this feature is washed out (not shown). Note that for the parameters of panel (b) also $\Omega_J \approx 0.024$ is finite but quite small.

For the doped system $n = 0.6$ and a quench $U_i = -1.0 \to U_F = -2.0$ it is the excitation energy Ω_J which now fits to the transition between two peaky structures in the DOS [panel (c)]. For larger quenches Ω_J decreases and does not appear any more in the DOS [panel (d)].

[1] C. A. Regal, M. Greiner, and D. S. Jin, Phys. Rev. Lett. **92**, 040403 (2004).
[2] M. W. Zwierlein, C. A. Stan, C. H. Schunck, S. M. F. Raupach, A. J. Kerman, and W. Ketterle, Phys. Rev. Lett. **92**, 120403 (2004).
[3] M. Bartenstein, A. Altmeyer, S. Riedl, S. Jochim, C. Chin, J. H. Denschlag, and R. Grimm, Phys. Rev. Lett. **92**, 203201 (2004).
[4] C. Chin, R. Grimm, P. Julienne, and E. Tiesinga, Rev. Mod. Phys. **82**, 1225 (2010).
[5] A. Behrle, T. Harrison, J. Kombe, K. Gao, M. Linkl, J.-S. Bernier, C. Kollath, and M. Köhl, Nat. Phys. **14**, 781 (2018).
[6] B. Mansart, J. Lorenzana, A. Mann, A. Odeh, M. Scarongella, M. Chergui, and F. Carbone, Proc. Natl. Acad. Sci. **110**, 4539 (2013).
[7] R. Matsunaga, Y. I. Hamada, K. Makise, Y. Uzawa, H. Terai, Z. Wang, and R. Shimano, Phys. Rev. Lett. **111**, 057002 (2013).
[8] R. Matsunaga, N. Tsuji, H. Fujita, A. Sugioka, K. Makise, Y. Uzawa, H. Terai, Z. Wang, H. Aoki, and R. Shimano, Science **345**, 1145 (2014).
[9] J. Bünemann and G. Seibold, Phys. Rev. B **96**, 245139 (2017).
[10] H. P. Ojeda Collado, G. Usaj, J. Lorenzana, and C. A. Balseiro, Phys. Rev. B **99**, 174509 (2019).
[11] M. Udina, T. Cea, and L. Benfatto, Phys. Rev. B **100**, 165131 (2019).
[12] M. Mootz, J. Wang, and I. E. Perakis, Phys. Rev. B **102**, 054517 (2020).
[13] T. Papenkort, V. M. Axt, and T. Kuhn, Phys. Rev. B **76**, 224522 (2007).

[14] T. Papenkort, T. Kuhn, and V. M. Axt, Phys. Rev. B **78**, 132505 (2008).
[15] H. Krull, D. Manske, G. S. Uhrig, and A. P. Schnyder, Phys. Rev. B **90**, 014515 (2014).
[16] P. W. Anderson, Phys. Rev. **112**, 1900 (1958).
[17] R. A. Barankov, L. S. Levitov, and B. Z. Spivak, Phys. Rev. Lett. **93**, 160401 (2004).
[18] E. A. Yuzbashyan, B. L. Altshuler, V. B. Kuznetsov, and V. Z. Enolskii, J. Phys. A: Math. Gen. **38**, 7831 (2005).
[19] R. A. Barankov and L. S. Levitov, Phys. Rev. Lett. **96**, 230403 (2006).
[20] E. A. Yuzbashyan, O. Tsyplyatyev, and B. L. Altshuler, Phys. Rev. Lett. **96**, 097005 (2006).
[21] E. A. Yuzbashyan and M. Dzero, Phys. Rev. Lett. **96**, 230404 (2006).
[22] M. Randeria and E. Taylor, Annu. Rev. Condens. Matter Phys. **5**, 209 (2014).
[23] S. Jochim, M. Bartenstein, A. Altmeyer, G. Hendl, S. Riedl, C. Chin, J. Hecker Denschlag, and R. Grimm, Science **302**, 2101 (2003).
[24] M. Greiner, C. A. Regal, and D. S. Jin, Nature (London) **426**, 537 (2003).
[25] M. W. Zwierlein, C. A. Stan, C. H. Schunck, S. M. F. Raupach, S. Gupta, Z. Hadzibabic, and W. Ketterle, Phys. Rev. Lett. **91**, 250401 (2003).
[26] T. Bourdel, L. Khaykovich, J. Cubizolles, J. Zhang, F. Chevy, M. Teichmann, L. Tarruell, S. J. J. M. F. Kokkelmans, and C. Salomon, Phys. Rev. Lett. **93**, 050401 (2004).
[27] C. Chin, M. Bartenstein, A. Altmeyer, S. Riedl, S. Jochim, J. Hecker Denschlag, and R. Grimm, Science **305**, 1128 (2004).
[28] A. Schirotzek, Y.-i. Shin, Christian H. Schunck, and W. Ketterle, Phys. Rev. Lett. **101**, 140403 (2008).
[29] L. W. Clark, L.-C. Ha, C.-Y. Xu, and C. Chin, Phys. Rev. Lett. **115**, 155301 (2015).
[30] R. S. Markiewicz, J. Lorenzana, G. Seibold, and A. Bansil, Phys. Rev. B **81**, 014509 (2010).
[31] J Bünemann, M. Capone, J. Lorenzana, and G. Seibold, New J. Phys. **15**, 053050 (2013).
[32] M. Schiró and M. Fabrizio, Phys. Rev. Lett. **105**, 076401 (2010).
[33] M. Schiró and M. Fabrizio, Phys. Rev. B **83**, 165105 (2011).
[34] G. Seibold and J. Lorenzana, Phys. Rev. Lett. **86**, 2605 (2001).
[35] G. Seibold, F. Becca, and J. Lorenzana, Phys. Rev. B **67**, 085108 (2003).
[36] G. Seibold, F. Becca, P. Rubin, and J. Lorenzana, Phys. Rev. B **69**, 155113 (2004).
[37] G. Seibold, F. Becca, and J. Lorenzana, Phys. Rev. Lett. **100**, 016405 (2008); Phys. Rev. B **78**, 045114 (2008).
[38] S. Ugenti, M. Cini, G. Seibold, J. Lorenzana, E. Perfetto, and G. Stefanucci, Phys. Rev. B **82**, 075137 (2010).
[39] M. Sandri and M. Fabrizio, Phys. Rev. B **88**, 165113 (2013).
[40] G. Mazza, Phys. Rev. B **96**, 205110 (2017).
[41] G. Seibold and J. Lorenzana, Phys. Rev. Lett. **94**, 107006 (2005).
[42] G. Seibold and J. Lorenzana, Phys. Rev. B **73**, 144515 (2006).
[43] G. Seibold and J. Lorenzana, Phys. Rev. B **80**, 012509 (2009).
[44] A. Georges, G. Kotliar, W. Krauth, and M. J. Rozenberg, Rev. Mod. Phys. **68** (1996).
[45] J. Lorenzana, G. Seibold, and R. Coldea, Phys. Rev. B **72**, 224511 (2005).
[46] M. Eckstein, M. Kollar, and P. Werner, Phys. Rev. Lett. **103**, 056403 (2009).
[47] P. Werner, N. Tsuji, and M. Eckstein, Phys. Rev. B **86**, 205101 (2012).
[48] N. Tsuji, M. Eckstein, and P. Werner, Phys. Rev. Lett. **110**, 136404 (2013).
[49] K. Balzer, F. A. Wolf, I. P. McCulloch, P. Werner, and M. Eckstein, Phys. Rev. X **5**, 031039 (2015).
[50] M. Sandri, M. Schiró, and M. Fabrizio, Phys. Rev. B **86**, 075122 (2012).
[51] G. Mazza and M. Fabrizio, Phys. Rev. B **86**, 184303 (2012).
[52] H. P. O. Collado, J. Lorenzana, G. Usaj, and C. A. Balseiro, Phys. Rev. B **98**, 214519 (2018).
[53] H. P. Ojeda Collado, G. Usaj, J. Lorenzana, and C. A. Balseiro, Phys. Rev. B **101**, 054502 (2020).
[54] R. Micnas, J. Ranninger, and S. Robaszkiewicz, Rev. Mod. Phys. **62**, 113 (1990).
[55] G. A. Medina, J. Simonin, and M. D. Núñez Regueiro, Phys. Rev. B **43**, 6206 (1991).
[56] J. O. Sofo and C. A. Balseiro, Phys. Rev. B **45**, 377 (1992).
[57] W. F. Brinkman and T. M. Rice, Phys. Rev. B **2**, 4302 (1970).
[58] A. F. Volkov and Sh. M. Kogan, Zh. Eksp. Teor. Fiz. **65**, 2038 (1973) [Sov. Phys. JETP **38**, 1018 (1974)].
[59] J. Bauer, A. C. Hewson, and N. Dupuis, Phys. Rev. B **79**, 214518 (2009).
[60] C. P. Slichter, *Principles of Magnetic Resonance*, Springer Series in Solid-State Sciences Vol. 1 (Springer, Berlin, 1990), p. 655.
[61] C. Shao, T. Tohyama, H.-G. Luo, and H. Lu, Phys. Rev. B **93**, 195144 (2016).
[62] D. J. Scalapino, S. R. White, and S. Zhang, Phys. Rev. B **47**, 7995 (1993).
[63] R. Shimano and N. Tsuji, Annu. Rev. Condens. Matter Phys. **11**, 103 (2020).
[64] J. Demsar, J. Low Temp. Phys. (2020), doi: 10.1007/s10909-020-02461-y.